12-1-2001

One-gas Models with Height-dependent Mean Molecular Weight: Effects on Gravity Wave Propagation

R. L. Walterscheid
The Aerospace Corporation

Michael P. Hickey Ph.D.
Embry-Riddle Aeronautical University, hicke0b5@erau.edu

Scholarly Commons Citation

Walterscheid, R. L., and M. P. Hickey (2001), One-gas models with height-dependent mean molecular weight: Effects on gravity wave propagation, J. Geophys. Res., 106(A12), 28831–28839, doi: https://doi.org/10.1029/2001JA000102

JOURNAL OF GEOPHYSICAL RESEARCH, VOL. 106, NO. A12, PAGES 28,831–28,839, DECEMBER 1, 2001

One-gas models with height-dependent mean molecular weight: Effects on gravity wave propagation

R. L. Walterscheid
Space Science Applications Laboratory, The Aerospace Corporation, Los Angeles, California, USA

M. P. Hickey
Department of Physics and Astronomy, Clemson University, Clemson, South Carolina, USA

Abstract. Many models of the thermosphere employ the one-gas approximation where the governing equations apply only to the total gas and the physical properties of the gas that depend on composition (mean molecular weight and specific heats) are height-dependent. It is further assumed that the physical properties of the gas are locally constant; thus motion-induced perturbations are nil. However, motion in a diffusively separated atmosphere perturbs local values of mean molecular weight and specific heats. These motion-induced changes are opposed by mutual diffusion of the constituent gases, which attempts to restore diffusive equilibrium. Assuming that composition is locally constant is equivalent to assuming that diffusion instantaneously damps the changes that winds attempt to produce. This is the limit of fast diffusion. In the limit of slow diffusion, gas properties are constant (conserved) following the motion but are perturbed locally by advection. An analysis of the static stability shows that composition effects significantly change the static stability, with greater changes for the slow-diffusion limit than for the fast-diffusion limit. We have used a one-gas full-wave model to examine the effects of wave-perturbed composition on gravity waves propagating through the lower thermosphere. We have augmented the conventional system (fixed gas properties) with predictive equations for composition-dependent gas properties. These equations include vertical advection and mutual diffusion. The latter is included in parameterized form as second-order scale-dependent diffusion. We have found that the fast diffusion implied by locally fixed properties has a significant effect on the dynamics. Predicted temperatures are larger for locally fixed composition than for conserved composition. The simulations with parameterized mutual diffusion gave results that are much closer to the results for conserved gas properties than for fixed properties. We found that the divergence between the fast and slow limits was greatest for fast waves and for colder thermospheres. This is because the propagation characteristics of fast waves are sensitive to changes in the static stability and because compositional gradients are stronger for colder thermospheres. We conclude that future models that use the one-gas approximation for fast waves in the lower thermosphere should include, at minimum, the simplification of conserved rather than fixed properties, especially for colder thermospheres.

1. Introduction

A widely used simplification in dynamical models of the diffusively stratified thermosphere is the application of equations for a single gas (the total gas) with height-dependent physical properties such as mean molecular weight and specific heats. A further approximation is that composition remains fixed despite the advection of one species relative to another [e.g., *Richmond and Matsushita*, 1975; *Fuller-Rowell and Rees*, 1981; *Mikkelsen et al.*, 1981; *Walterscheid et al.*, 1985; *Mikkelsen and Larsen*, 1991; *Brinkman et al.*, 1995; *Hagan et al.*, 1999]. This approximation is used in lieu of the much more complicated and computationally intensive system of equations that must be solved when a multiconstituent approach is used [e.g., *Colegrove et al.*, 1966; *Hays et al.*, 1973; *Reber and Hays*, 1973; *Straus et al.*, 1977; *Mayr et al.*, 1978; *Del Genio et al.*, 1979; *Dickinson et al.*, 1984; *Sun et al.*, 1995]. A general result is that motion (primarily vertical motion) drives a diffusively separated atmosphere with height-dependent composition out of diffusive equilibrium and causes composition to be locally perturbed. The implications of local composition perturbations for gravity wave propagation is the primary subject of this study.

Figure 1 shows the profile of mean molecular weight obtained from the extended Mass Spectrometer Incoherent Scatter (MSIS) model [*Hedin*, 1991] for moderate solar and geomagnetic conditions ($Ap = 10$, $F_{10.7} = 150$) at latitude 40°N and 0600 LT for January 15. We denote this profile the warm midlatitude (W-ML) profile. Also shown is the profile for an auroral latitude (70°N) for quiet conditions ($Ap = 0$, $F_{10.7} = 70$) for January 15. We denote this the cold high-latitude (C-HL) profile. The W-ML profile shows nearly constant mean molecular weight up to the homopause (located near 100 km), where $\bar{M} = 28.3$ kg kmol^{-1}. Above this altitude, gases begin to separate diffusively, with the concentrations of the heavier

Paper number 2001JA000102.
0148-0227/01/2001JA000102$09.00

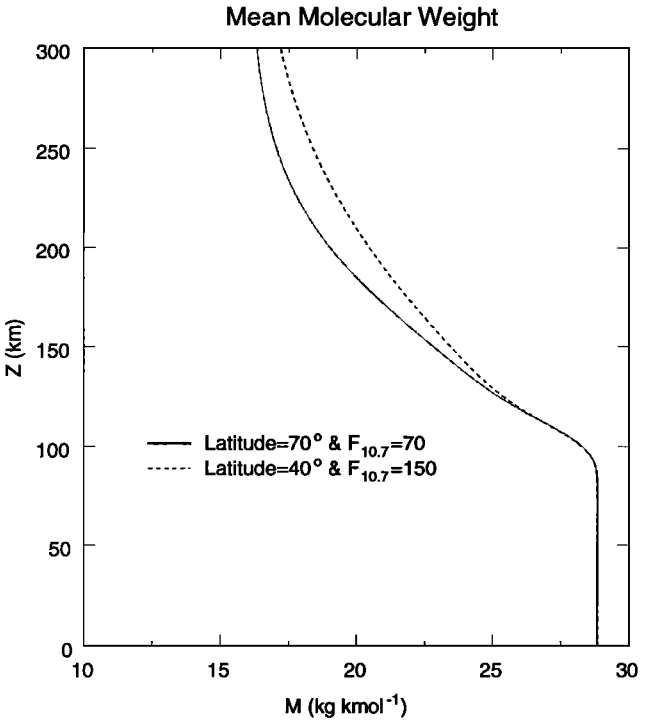

Figure 1. Profile of mean molecular weight obtained from the extended Mass Spectrometer Incoherent Scatter (MSIS) model [*Hedin*, 1991] for moderate solar and geomagnetic conditions ($Ap = 10, F_{10.7} = 150$) at latitude 40°N and 0600 LT for January 15. Also shown is the profile for an auroral latitude (70°N) for quiet conditions ($Ap = 0, F_{10.7} = 70$) for January 15.

gases falling off more rapidly than the concentrations of the lighter gases, causing the relative concentration of the lighter gases to increase with altitude. Just above ~100 km, $\bar{M}$ begins a fairly steep decrease, reflecting both the onset of diffusive separation and the photodissociation of molecular oxygen. By ~130 km, $\bar{M}$ has decreased by 3 kg kmol^{-1} to ~25 kg kmol^{-1}. Above ~130 km the decrease slows and over the next 70 km decreases by another 4.5 units, giving $\bar{M} \approx 20.5$ kg kmol^{-1} at 200 km. Above ~200 km the mixture is dominated by atomic oxygen ($M_O = 16$ kg kmol^{-1}) and the decrease continues to slow. Over the next 100 km, $\bar{M}$ falls just another 3 kg kmol^{-1} to 17.3 kg kmol^{-1} near 300 km. At greater altitudes (not shown), even lighter gases (He and H) become increasingly important and eventually dominate. The C-HL profile is similar except that the initial decrease is more rapid, decreasing to ~19 kg kmol^{-1} by 200 km. The divergence between the two profiles is maximum ~230 km, where the difference attains ~1.6 kg kmol^{-1}. Above ~230 km the decrease in the C-HL $\bar{M}$ profile slows relative to the W-ML profile so that by 300 km the difference is reduced to ~1 kg kmol^{-1}. The more rapid decrease of $\bar{M}$ with altitude above the homopause at high latitudes is explained by the increased rate at which heavy species concentrations diminish relative to light species concentrations in colder atmospheres, the increased rate being a result of the smaller scale heights of the heavy species. We perform calculations primarily for the auroral latitude because compositional effects are greater and because high latitudes are the scene of prolific wave generation, both in the lower atmosphere and in the aurora [*Theon et al.*, 1967; *Balsley et al.*, 1984].

The specific heats increase as the relative abundance of lighter species increases, but the change with altitude is less pronounced. For the W-ML profile the fractional change at 200 km in $\bar{c}_p$ relative to its value at 100 km is ~14%, compared with ~−27% for $\bar{M}$, while for the C-HL profile the respective values are 18% for $\bar{c}_p$ compared with 33% for $\bar{M}$.

In the conventional one-gas approximation, total-gas molecular weight and specific heats are assumed to be locally constant; they are not perturbed by dynamics. However, motion (particularly vertical motion) perturbs composition. Diffusion acts to damp the perturbed composition. The conventional one-gas approximation is equivalent to assuming that diffusion acts so fast that it instantaneously annuls the changes that dynamics attempts to produce. In the other limit (slow diffusion), composition is conserved following the motion but is locally perturbed.

In the following sections we discuss the competing effects of dynamics and diffusion and the implications of fixed composition in one-gas models and present numerical results for different assumptions regarding the rate at which diffusion damps wave disturbances in composition.

2. Theory

It is easily shown (see Appendix A) that

$$\frac{D \log M}{Dt} = \frac{\partial \log M}{\partial t} + w \frac{\partial \log M}{\partial z} = \frac{1}{N} \sum_i \nabla \cdot \mathbf{\Phi}_i, \quad (1)$$

and thus

$$\frac{\partial \log M}{\partial t} = -w \frac{\partial \log M}{\partial z} + \frac{1}{N} \sum_i \nabla \cdot \mathbf{\Phi}_i, \quad (2)$$

where N is total gas number density, w is the vertical velocity, t is time, and z is the vertical coordinate. For simplicity, we have ignored the effects of horizontal advection which should usually be small compared with vertical advection. In this study we are interested in the perturbing effects of waves. The perturbation form of (2) is

$$\frac{\partial}{\partial t} \frac{M'}{\bar{M}} = -w' \frac{\partial \log \bar{M}}{\partial z} + \frac{1}{\bar{N}} \sum_i \nabla \cdot \mathbf{\Phi}_i', \quad (3)$$

where overbars refer to an average with respect to a horizontal coordinate and primes refer to a deviation therefrom. We have assumed a basic state of rest. The quantity $\mathbf{\Phi}_i = \mathbf{v}_i n_i - \mathbf{v} n_i$, where $\mathbf{v}_i$ is the velocity of the ith constituent, $\mathbf{v}$ is the mass-weighted velocity of the total gas, and n_i is the number density of the ith species. Thus $\mathbf{\Phi}_i$ is the flux of n_i by $\mathbf{v}_i$ relative to the flux by $\mathbf{v}$ [*Hays et al.*, 1973]. In obtaining (3), it has been assumed that the background state is in diffusive equilibrium, and thus $\bar{\mathbf{\Phi}}_i = 0$.

The first term on the right side of (3) represents the perturbing effect of dynamics, while the second term represents the restoring effect of diffusion. As mentioned, there are two limiting cases of interest: the limits of fast and slow diffusion. In the former, diffusion acts so fast that it instantaneously damps the changes winds attempt to produce, whence $\partial M'/\partial t = 0$. For steady waves, $\partial M'/\partial t = i\omega M'$ and $M' = 0$. In the latter limit, diffusion acts too slowly to damp the wave-

caused perturbation, whence $DM/Dt = 0$ (M is conserved following the motion).

Fuller-Rowell and Rees [1987] have evaluated compositional effects in a one-gas model of the neutral response to auroral forcing. This was done for the total-gas velocity defined as a number density weighting of individual species velocities, rather than the mass density weighting that avoids a collisional term in both the total-gas momentum and mass density equations. In order to avoid the considerable complications arising from these terms, we adopt another approach for evaluating mutual diffusion effects on wave propagation.

We use an approach based on Newtonian damping to evaluate the effects of mutual diffusion in restoring diffusive equilibrium. We assume that the damping is proportional to the departure from static equilibrium M'; thus

$$\frac{1}{\bar{N}} \sum_i \nabla \cdot \mathbf{\Phi}_i' \sim -\alpha M' \tag{4}$$

and α is a damping coefficient with units of s^{-1}. The evaluation of α must involve the mutual diffusion coefficients with units of $m\ s^{-2}$ and some quantity with the dimensions of inverse length squared. A reasonable choice for the latter quantity is the vertical scale of the wave L_z. It is the inverse vertical wave number when the wave is purely vertically propagating, and it is the inverse e-folding attenuation depth when the wave is purely evanescent. More generally, it is the inverse complex vertical wave number (refractive index). In the region of interest the gas is dominated by O, O_2, and N_2. The mutual diffusion coefficient for each of these gases through the others is similar, and we use a single value D, whence $\alpha \sim D/L_z^2$ (U.S. Standard Atmosphere, 1976). The limiting case of fast diffusion corresponds to $\alpha \to \infty$, and the limiting case of slow diffusion corresponds to $\alpha \to 0$.

Our numerical approach is to evaluate L_z^{-2} as $L_z^{-2} = \partial^2/\partial z^2$ and implement damping in terms of second-order scale-dependent diffusion as

$$\frac{1}{\bar{N}} \sum_i \nabla \cdot \mathbf{\Phi}_i' = D \frac{\partial^2}{\partial z^2} M'. \tag{5}$$

Using (5) in (3) gives the prognostic equation for M':

$$\frac{\partial}{\partial t} \frac{M'}{\bar{M}} = -w' \frac{\partial \log \bar{M}}{\partial z} + \frac{D}{\bar{M}} \frac{\partial^2}{\partial z^2} M'. \tag{6}$$

In the same spirit,

$$\frac{\partial}{\partial t} \frac{c_p'}{\bar{c}_p} + w' \frac{\partial \log \bar{c}_p}{\partial z} = \frac{D}{\bar{c}_p} \frac{\partial^2}{\partial z^2} c_p'. \tag{7}$$

We examine the dynamical effects of composition by examining the density fluctuation and parcel buoyancy. The linearized ideal gas law is

$$\frac{\rho'}{\bar{\rho}} = \frac{P'}{\bar{P}} - \frac{T'}{\bar{T}} + \frac{M'}{\bar{M}} \approx -\frac{T'}{\bar{T}} + \frac{M'}{\bar{M}}, \tag{8}$$

where the approximation is valid for typical gravity waves and is the usual approximation for evaluating parcel buoyancy. The linearized first law is

$$\frac{\partial}{\partial t} \frac{T'}{\bar{T}} + \frac{\bar{N}_0^2}{g} w = \alpha \frac{c_p'}{\bar{c}_p}, \tag{9}$$

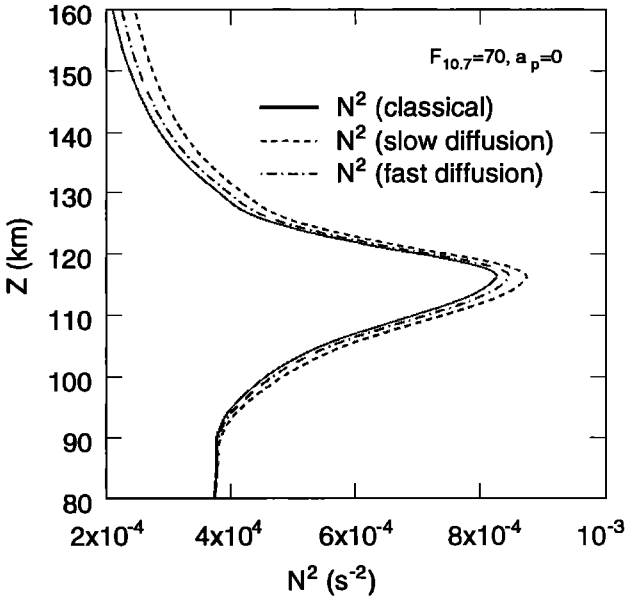

Figure 2. The vertical profiles of Brunt-Väisälä frequency for the limiting cases of slow and fast diffusion based on auroral $\bar{M}$ and $\bar{c}_p$ profiles. Also plotted is the classical Brunt-Väisälä frequency N_0^2 where compositional effects are ignored.

where $\bar{N}_0^2 = g\partial \log \bar{\theta}/\partial z$ and θ is potential temperature and where $D\partial^2( )/\partial z^2 = -\alpha( )$. The quantity $\bar{N}_0$ is the constant-composition form of the Brunt-Väisälä frequency. Assuming waveform solutions in (9) and (7) and again using (7) gives

$$\frac{T'}{\bar{T}} = -\left(\frac{\bar{N}_0^2}{g} + \frac{\alpha}{i\omega + \alpha} \frac{\partial \log \bar{c}_p}{\partial z}\right) \zeta, \tag{10}$$

where $\zeta = w'/i\omega$ is the Eulerian estimate of vertical displacement. Using (10) in (8) and evaluating $M'/\bar{M}$ by means of (6) with α evaluated as above gives

$$-g \frac{\rho'}{\bar{\rho}} = -\left(\bar{N}_0^2 + \frac{g\alpha}{i\omega + \alpha} \frac{\partial \log \bar{c}_p}{\partial z} - \frac{gi\omega}{i\omega + \alpha} \frac{\partial \log \bar{M}}{\partial z}\right) \zeta, \tag{11}$$

where the left-hand side is the buoyancy force and the expression in parentheses may be interpreted as a buoyancy frequency modified by compositional effects. For the fast-diffusion limit (whence M' and $c_p' \to 0$),

$$-g \frac{\rho'}{\bar{\rho}} = -\left(\bar{N}_0^2 + g \frac{\partial \log \bar{c}_p}{\partial z}\right) \zeta, \tag{12}$$

and for the slow-diffusion limit (whence M and c_p are conserved),

$$-g \frac{\rho'}{\bar{\rho}} = -\left(\bar{N}_0^2 - g \frac{\partial \log \bar{M}}{\partial z}\right) \zeta. \tag{13}$$

Figure 2 shows the vertical profiles of Brunt-Väisälä frequency for the two limiting cases based on auroral $\bar{M}$ and $\bar{c}_p$ profiles. Also plotted is the classical Brunt-Väisälä frequency $\bar{N}_0^2$, where compositional effects included in the additional terms in (12) and (13) are ignored. The compositional contribution to the Brunt-Väisälä frequency is greatest for slow diffusion. For slow diffusion, composition contributes to an increase in the square of the Brunt-Väisälä frequency at all altitudes above ~90 km.

The effect is greatest at the peak of the profile in the lower thermosphere just below 120 km and at higher altitudes above ~130 km. The fractional change at the peak is ~6%, and at altitudes above ~140 km it is ~18%. For fast diffusion, composition also contributes to an increase relative to $\bar{N}_0^2$. The contribution is smaller, about half that due to $\bar{M}$ at the peak. The divergence between the fast and slow limits is greatest at the higher altitudes plotted, with the increase over $\bar{N}_0^2$ for the slow limit being ~2 times greater than for the fast limit.

The compositional effects on static stability can be significant. The greatest effects should be on waves that have long vertical scales, as these waves are most sensitive to changes in the static stability leading to changes in the vertical wave number [*Walterscheid et al.*, 1999, 2000]. A special class of waves in this category are the waves that are ducted or partially ducted in the region of the Brunt-Väisälä maximum in the lower thermosphere [*Walterscheid et al.*, 1999].

The effects of composition on static stability in the two limits (equations (12) and (13)) may be explained as follows. In the fast-diffusion limit, $M' \rightarrow 0$ and variable mean molecular weight has no effect through (8). This is explained further below. Also, $c_p' \rightarrow 0$, but the limit of $\alpha c_p'$ does not $\rightarrow 0$ as $\alpha \rightarrow 0$. In this limit, (9) becomes

$$\frac{T'}{\bar{T}} + \frac{\partial \log \bar{c}_p}{\partial z}\zeta = -\frac{\bar{N}_0^2}{g}\zeta. \tag{14}$$

The left side of (14) represents the fractional change in a parcel's enthalpy that occurs when a parcel is displaced vertically subject to fast diffusion. The enthalpy change driven by the term on the right is divided between the two terms on the left. Since $\partial \log \bar{c}_p/\partial z > 0$, an upward displacement results in an increase in the parcel's enthalpy. This is compensated by increased cooling relative to constant composition, which increases the rate of density decrease and increases the downward restoring force. This explains the increase in the Brunt-Väisälä frequency according to (12). When the slow-diffusion limit applies, but the fast-diffusion limit is implicitly invoked by using fixed composition, the second term on the left side of (14) becomes a spurious heat source, or alternatively a spurious source of buoyancy.

In the slow-diffusion limit, specific heat is conserved and the right sides of (9) and (14) are zero. Then the effects of variable M enter through the second term on the right side of (8). This term represents the fact that the density disturbance is increased by having the displaced parcel move to where the environmental air has a greater abundance of light species than the parcel itself. Since $\partial \log \bar{M}/\partial z < 0$, this occurs for an upward displaced parcel. This means that the parcel is heavier relative to the displaced air than it would be were composition constant with altitude; thus the parcel experiences an increased downward restoring force. This explains the increase in the Brunt-Väisälä frequency according to (13). It also explains why the limit of fast diffusion does not include this effect; since then, as in the constant composition case, the parcel and the environment have the same composition.

For fixed displacement the amplitude of $\rho'/\bar{\rho}$ should be greater for conserved composition than for locally fixed composition (see equations (12) and (13)). However, it is clear that for the same initial heating, parcel excursions should be increased by reduced buoyancy (as measured by N^2) since the restoring force on buoyant parcels is less. Physically, the buoyant effect on upward displaced parcels of mixing in lighter constituents is the same as adding heat. Thus we expect the net effect of the rapid mixing implied by fixed composition is to increase parcel displacement and thus wave amplitude.

3. Augmented Full-Wave Model

We have simulated the composition effects using the full-wave model described by *Hickey et al.* [2000, and references therein] augmented with (6) and (7) and the $M'/\bar{M}$ term in the ideal gas law. The model includes rotation and scale-dependent dissipation by molecular and eddy viscosity and heat conduction. The diffusion coefficient D appearing in (6) and (7) is obtained from the U.S. Standard Atmosphere (1976). The coefficient is for the diffusion of O through O_2 and N_2. Profiles of M and c_p are obtained from the MSIS90-E model. The values of $\bar{c}_p$ used in the model are calculated from composition according to *Banks and Kockarts* [1973, equation (14.15)]. The mean value of $\bar{c}_p$ is obtained by first calculating the ratio of specific heats $\gamma = c_p/c_v$ using the number density weighted degrees of freedom [see *Banks and Kockarts*, 1973, equations (14.14) and (14.13)] and then deducing $\bar{c}_p$ from $c_p = R + c_v$ and $c_p = \gamma c_v$.

In the full-wave model the altitude variation of the forcing is a Gaussian function centered on 20 km altitude with a full width at half maximum of 0.1 km. The magnitude of the forcing is the same for all waves although the actual value is arbitrary. No attempt was made to rescale the results to match measured amplitudes. The important aspect of the simulations is the relative difference between simulations as a function of the rate of mutual diffusion, which in our linear model is independent of wave amplitude.

4. Model Results and Discussion

In this section we present the results of simulations for long- and short-period gravity waves. We also present an equivalent gravity wave calculation of a semidiurnal tidal mode [*Lindzen*, 1970].

4.1. Gravity Wave Calculations

Calculations were performed for the C-HL profile for two wave periods: 10 and 60 min. The horizontal wavelength for the 10-min wave is 60 km, giving a horizontal phase speed of 100 m s^{-1}. This wave resembles the faster quasi-monochromatic waves observed in airglow imagers. The wavelengths for the 1-hour waves range from 240 to 720 km, corresponding to phase speeds from 50 to 200 m s^{-1}. Waves with order hour periods are the energy-containing waves of the spectrum. Calculations were done for the five-equation model set, wherein composition is kept locally fixed (the usual one-gas approach), and for the augmented seven-equation set, wherein composition is conserved following the motion. To reiterate, the former is the fast-diffusion limit while the latter is the slow-diffusion limit. (Note that the slow limit can also be implemented by simply taking the specific heats outside of the substantial derivative and adding one equation for the wave-perturbed mean molecular weight. We use a seven-equation set to enable calculations based on (5) and (7).)

A separate calculation was done for the W-ML profile that demonstrates that the slow-diffusion limit is a good approximation in the lower thermosphere. Figure 3 shows the amplitude of the temperature wave for a wave with horizontal wavelength λ = 540 km and period τ = 60 min for the fast- and slow-diffusion limits and for the diffusion coefficients based on

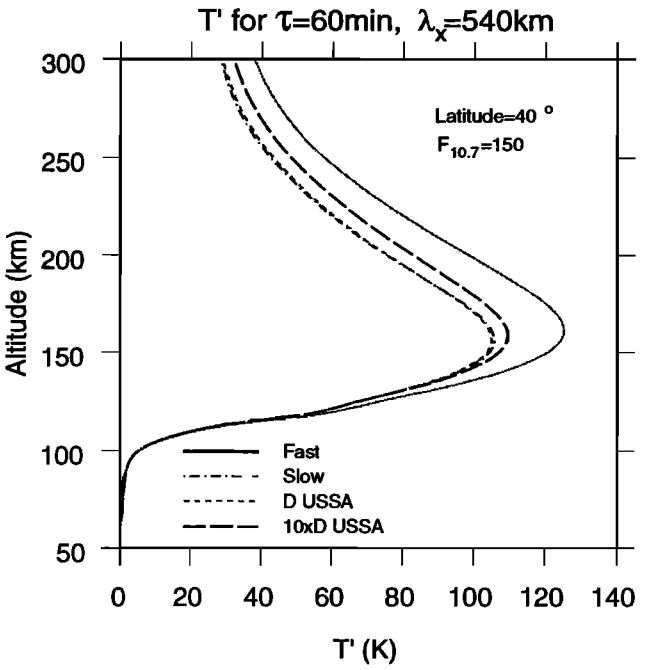

Figure 3. The amplitude of the temperature wave versus altitude for a horizontal wavelength λ = 540 km and period τ = 60 min for the fast- and slow-diffusion limits and for the diffusion coefficients based on U.S. Standard Atmosphere (1976). Also shown are results for the same coefficients increased by a factor of 10.

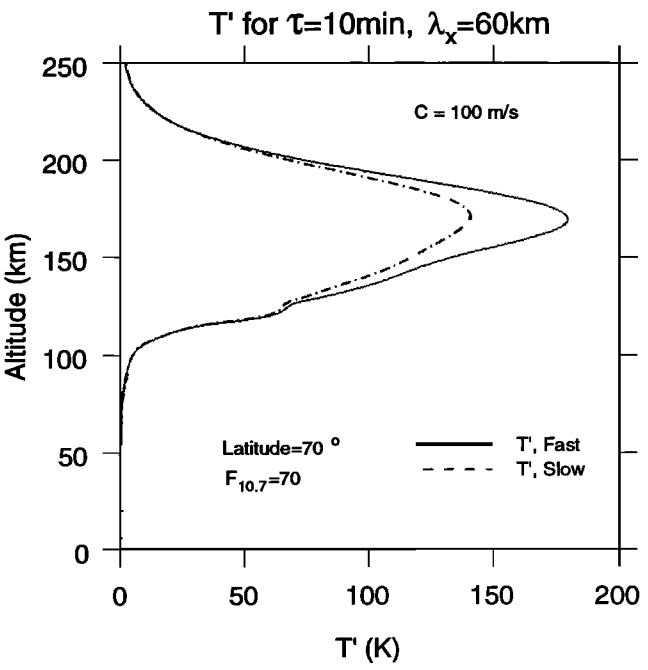

Figure 4. The calculated temperature amplitudes versus altitude for the fast and slow limits for a 10-min wave with a horizontal wavelength of 60 km. The calculations are for the high-latitude and low solar flux conditions.

U.S. Standard Atmosphere (1976). Also shown are results for the same coefficients increased by a factor of 10. The background atmosphere is based on the quiet-time auroral conditions given above. The wave for the fast-diffusion limit (solid curve) has the greatest amplitude, while the wave for the slow-diffusion limit has the smallest amplitude. The two curves based on D are significantly closer to the slow-diffusion limit than the fast-diffusion limit. This is, in part, a consequence of the long vertical scales associated with this wave. The gases flow through each other, but to little effect. We have found that for waves with short vertical scales there is little difference between the fast and slow limits, and the result based on D is necessarily close to the fixed-composition result. However, when the two limits diverge, the slow limit always resembles the results based on D much more closely than does the fast limit. Our approach for modeling the effects of mutual diffusion is heuristic but seems reasonable. Therefore we conclude that since the results for the slow-diffusion limit are not too different from even the results for 10 × D, the results for the slow-diffusion limit are accurate. Henceforward we will show only the fast- and slow-diffusion limits for 1-hour-period waves and shorter.

The remainder of this section refers to calculations for high-latitude conditions. We dwell on C-HL conditions but also refer to some warm high-latitude calculations for comparison. Figure 4 shows the calculated amplitudes for the fast and slow limits for a 10-min wave with a horizontal wavelength of 60 km. This wave is similar to waves seen in the airglow images that appear to be ducted or partially ducted in the lower thermosphere duct [*Isler et al.*, 1997; *Taylor et al.*, 1995; *Walterscheid et al.*, 2000; *Hecht et al.*, 2001]. However, no effort is made here to select a wave exhibiting such behavior [*Walterscheid et al.*, 1999]. The effects of local composition change included in the seven-equation set reduce the magnitude of the wave relative to the five-equation set, wherein local changes are zero. The largest differences occur near where wave amplitude peaks. The difference is a significant ~28% increase in amplitude as a result of fixed composition. The sensitivity to composition is a consequence of the wave being marginally evanescent or propagating in the upper mesosphere and lower thermosphere.

Figure 5 shows the amplitude of the fractional fluctuations in c_p, M, and T versus altitude for the slow limit for the wave shown in Figure 4. Also shown is the fractional change in T for the fast limit. The relative fluctuation in M is ~25% of the fluctuation in T for the slow limit and accounts for much of the difference between the fluctuations of T for the fast and slow limits. This is a fairly general result where the T' amplitude is governed mainly by adiabatic displacement. At higher altitudes the difference is governed more by the effects of static stability combined with scale-dependent dissipation. The amplitude of $c_p'/\bar{c}_p$ is shown for comparison. At most it is ~60% of $M'/\bar{M}$.

Figures 6–9 show the results for the 60-min wave for wavelengths of 180, 360, 540, and 720 km. As the horizontal wavelength λ_x increases, the waves peak progressively higher because the vertical wavelength increases and thus scale-dependent molecular dissipation decreases. For λ_x = 180 km the peak is located near 120 km altitude, while for λ_x = 720 km the main peak is near 175 km. The effects of composition change reduce the amplitude of waves relative to amplitudes calculated with fixed composition. The largest differences occur near where wave amplitudes peak. The size of the difference is a function of the sensitivity of the wave to composition-caused changes in the vertical structure of static stability. The sensitivity to changes in stability is greater for waves with longer vertical wavelengths (especially waves near evanescence). As is usually the case, the waves with faster phase

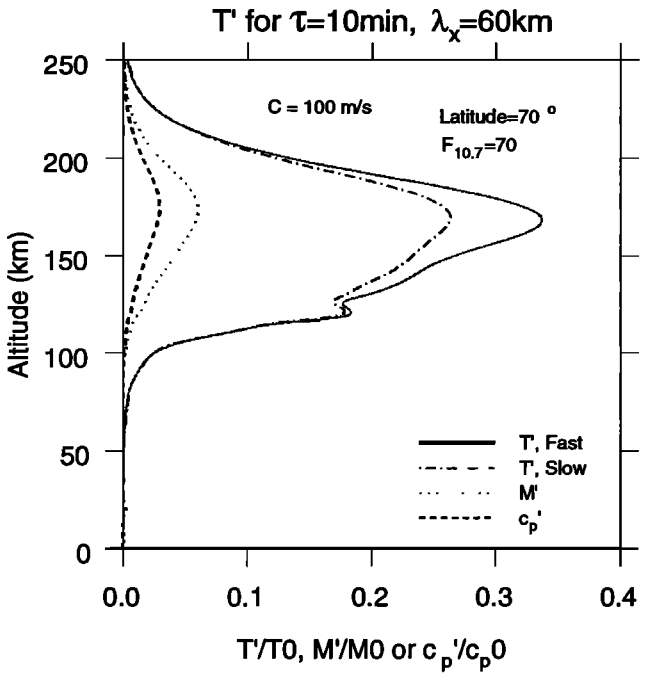

Figure 5. The amplitude of the fractional fluctuations in c_p, M, and T versus altitude for the slow limit for the wave shown in Figure 4. Also shown is the fractional chance in T for the fast limit.

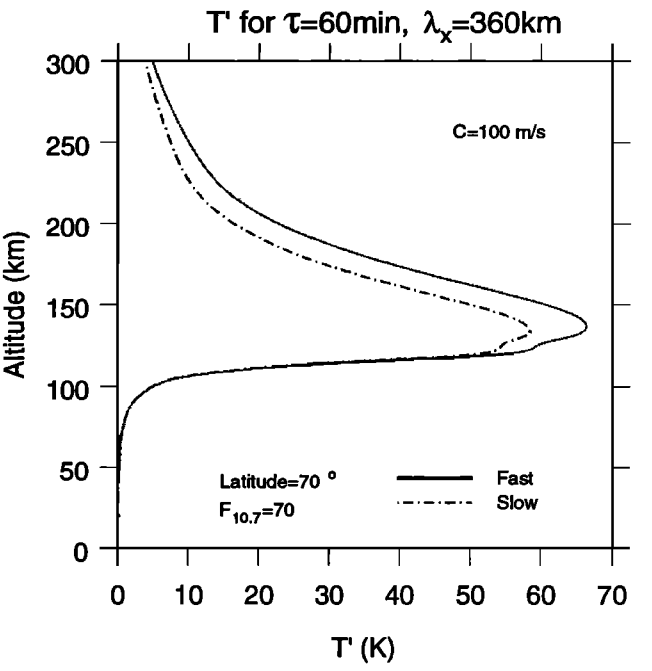

Figure 7. Same as Figure 6 except for a horizontal wavelength of 360 km.

speeds (longer horizontal wavelengths) have longer vertical wavelengths. The increasing wavelength sensitivity is seen in Figures 6–9. The fractional divergence between the slow and fast limits increases as the horizontal wavelength λ_x increases. For λ_x = 180 km the divergence is slight. For λ_x = 360 km the divergence referred to the slow limit is ~14% near the peak. For λ_x = 540 km the divergence is larger yet, and significant values exist over a much larger range of altitudes. In absolute terms, the divergence between solutions increases up to the amplitude peak near 160 km and remains fairly constant up to about 220 km, where it begins to decrease. By ~250 km the divergence is again fairly constant and remains so up to the highest altitude plotted (300 km). The fractional divergence near the peak is 22%. It increases to a maximum value of 34% near 220 km altitude. The results for the longest wavelength (λ_x = 720 km) are similar, with the divergence increasing up

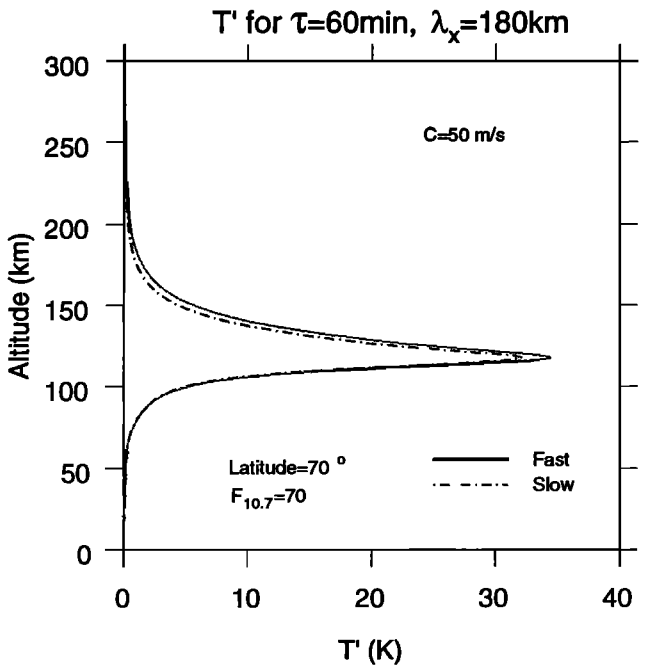

Figure 6. Same as Figure 4 except for a 60-min wave with a horizontal wavelength of 180 km.

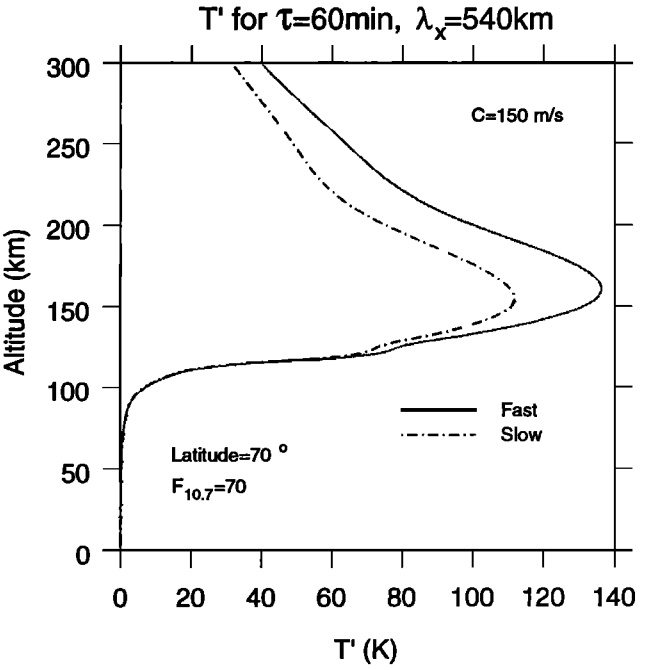

Figure 8. Same as Figure 6 except for a horizontal wavelength of 540 km.

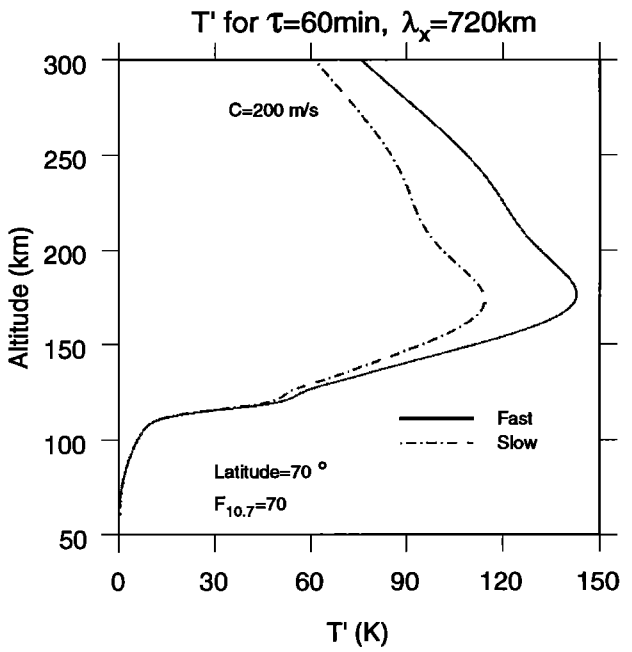

Figure 9. Same as Figure 6 except for a horizontal wavelength of 720 km.

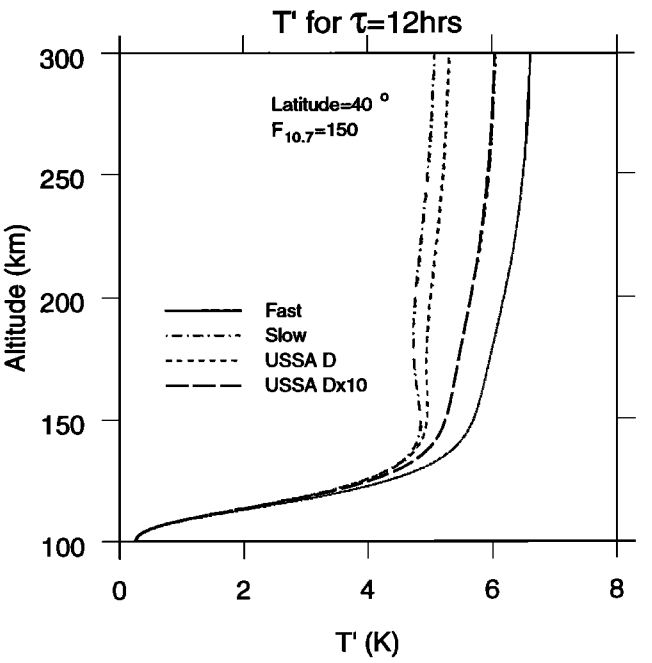

Figure 10. The amplitude of the temperature wave versus altitude for an equivalent gravity wave calculation of the semidiurnal 2,2 mode for the fast- and slow-diffusion limits and for the diffusion coefficients based on U.S. Standard Atmosphere (1976). Also shown are results for the same coefficients increased by a factor of 10.

to the amplitude maximum (located near 170 km) and decreasing between about 200 and 250 km. For this wave the fractional divergence near the peak is 25%, increasing to a maximum value of 31% near 220 km altitude. The general increase in the divergence between the slow and fast limits as horizontal wavelength (phase speed) increases reflects both decreased damping of the wave before compositional effects can accumulate and increased sensitivity of the solutions to differences in the refractive index gradients between the fast and slow limits as the vertical wavelength increases (tends toward evanescence).

It is also of interest to compare the 60-min $\lambda_x = 540$ km solution for the C-HL thermosphere (Figure 8) with solutions for a high-latitude warm thermosphere. Accordingly, we have also performed calculations (not shown) for 70°N for conditions where $F_{10.7} = 150$ and $Ap = 10$, which we denote W-HL. As expected, the divergence between the fast and slow limits is greater for C-HL than for the W-HL conditions in the lower thermosphere, where the C-HL vertical gradient of $\bar{M}$ is greater because of the scale-height sensitivity to temperature mentioned above. The divergence between solutions for the W-HL conditions resembles the divergence for the C-HL conditions shown in Figure 8. The main difference is that the absolute divergence does not significantly decrease above the amplitude peak for W-HL conditions (thus the fractional difference continues to increase). The fractional divergence (with respect to the slow limit) at the amplitude peak is 22% for the C-HL conditions and 14% for the W-HL conditions. The maximum fractional divergence for C-HL conditions is 34% and occurs near 220 km. The W-HL divergence at the same altitude is 30%. The maximum divergence for the W-HL atmosphere occurs near 280 km and has a value of 38%; the corresponding C-HL value is 27%. Calculations for $\lambda_x = 720$ km gave similar results.

4.2. Equivalent Gravity Wave Tidal Calculation

We have also performed a tidal calculation using an equivalent gravity wave model [*Lindzen*, 1970; *Richmond*, 1975]. In this model the horizontal wavelength and Coriolis parameter are adjusted to give maximal correspondence with a given tidal mode. We have performed a calculation for the semidiurnal 2,2 mode. This mode has long vertical scales and should exhibit sensitivity to composition change similar to the fast waves considered above. However, the fast limit should be more accurate because the timescale of the tide compared with the timescale α^{-1} for mutual diffusion is much longer than for the gravity waves. The calculation was done for an equinoctial midlatitude temperature profile based on the extended MSIS model. This profile was chosen as being more or less representative of the global mean temperature. The parameters of the model were obtained from *Richmond* [1975]. Mode coupling induced by viscosity and thermal conduction was ignored. The tide was forced in the same manner as the gravity waves: No attempt was made to include realistic tidal forcing. In view of the simplicity of the simulation the results can only give a general indication of the importance of compositional effects. Figure 10 shows the amplitude of the temperature wave for the equivalent gravity wave calculation of the semidiurnal 2,2 mode for the fast- and slow-diffusion limits and for the diffusion coefficients based on U.S. Standard Atmosphere (1976). Also shown are results for the same coefficients increased by a factor of 10. As expected, the effects of mutual diffusion are greater for the semidiurnal tide than for the faster waves considered previously. For diffusion rates 10 times nominal, the solution is closer to the fast limit than to the slower limit. However, for the nominal values the slow limit is clearly the more accurate. The fast and slow limits diverge significantly until ~175 km, where the fast limit attains a value ~29% larger than the slow limit. Above ~175 km the difference does not change much. These results indicate the likelihood that the

tidal calculation should include the effects of local composition change.

5. Summary and Conclusions

We have found that the fast damping of compositional perturbations by mutual diffusion implied by locally fixed properties has a significant effect on the dynamics. Predicted temperatures are significantly larger for locally constant composition than for conserved composition. Realistic values of mutual diffusion coefficients gave results much closer to the results for conserved properties than for fixed properties. We conclude that future models that use the one-gas approximation to model fairly fast waves in fairly cold lower thermospheres should include, at minimum, the simplification of conserved rather than fixed properties. This conclusion may apply as well to tides with long vertical scales. For other waves and other conditions, where wave reflection is not a significant factor affecting the wave vertical structure, the simple device of increasing the rate of molecular diffusion slightly might be sufficient. Finally, we remark that we have performed calculations for climatological atmospheres. Under disturbed conditions, high-latitude heating can lead to a large depletion of light species in the lower thermosphere, and under these conditions wave-induced compositional change may affect a broad range of waves, including comparatively slow waves [*Fuller-Rowell*, 1984; *Hecht et al.*, 1991].

Appendix A

Equation (1) is obtained as follows. The definition of mean molecular weight is

$$M = \frac{1}{N} \sum_i n_i M_i, \tag{A1}$$

where M_i is the molecular weight of the ith species. Differentiating (A1) with respect to time gives

$$\frac{DM}{Dt} = -\frac{1}{N^2}\frac{DN}{Dt} \sum_i n_i M_i + \frac{1}{N} \sum_i \frac{Dn_i}{Dt} M_i. \tag{A2}$$

Using individual specie and total-gas continuity equations [*Hays et al.*, 1973] gives

$$\frac{DM}{Dt} = -\frac{1}{N} \sum_i (M_i - M) \nabla \cdot \mathbf{\Phi}_i. \tag{A3}$$

By definition,

$$\sum_i M_i \mathbf{\Phi}_i = 0; \tag{A4}$$

whence

$$\frac{D \log M}{Dt} = \frac{1}{N} \sum_i \nabla \cdot \mathbf{\Phi}_i. \tag{A5}$$

Acknowledgments. Work at The Aerospace Corporation was supported by NASA grants NAG5-9193 and NAG5-4528. Work at Clemson University was supported by NSF grant ATM-9896276.

Janet G. Luhmann thanks David Fritts and another referee for their assistance in evaluating this paper.

References

Balsley, B. B., W. L. Ecklund, and D. C. Fritts, VHF echoes from the Arctic mesosphere and lower thermosphere, part I, Observations, in *Dynamics of the Middle Atmosphere*, edited by J. R. Holton and T. Matsuno, pp. 77–96, Terra Sci., Tokyo, 1984.

Banks, P. M., and G. Kockarts, *Aeronomy: Part B*, 355 pp., Academic, San Diego, Calif., 1973.

Brinkman, D. G., R. L. Walterscheid, L. R. Lyons, D. C. Kayser, and A. B. Christensen, *E* region neutral winds in the postmidnight diffuse aurora during the ARIA 1 rocket campaign, *J. Geophys. Res.*, *100*, 17,308–17,320, 1995.

Colegrove, F. D., F. S. Johnson, and W. B. Hanson, Atmospheric composition in the lower thermosphere, *J. Geophys. Res.*, *71*, 2227–2236, 1966.

Del Genio, A. D., G. Schubert, and J. M. Straus, Characteristics of acoustic-gravity waves in a diffusively separated atmosphere, *J. Geophys. Res.*, *84*, 1865–1879, 1979.

Dickinson, R. E., E. C. Ridley, and R. G. Roble, Thermospheric general circulation with coupled dynamics and composition, *J. Atmos. Sci.*, *41*, 205–219, 1984.

Fuller-Rowell, T. J., A two-dimensional, high-resolution, nested-grid model of the thermosphere, 1, Neutral response to an electric field "spike," *J. Geophys. Res.*, *89*, 2971–2990, 1984.

Fuller-Rowell, T. J., and D. Rees, A three-dimensional time-dependent simulation of the global dynamical response of the thermosphere to a geomagnetic substorm, *J. Atmos. Terr. Phys.*, *43*, 701–721, 1981.

Fuller-Rowell, T. J., and D. Rees, Conservation equation for mean molecular weight for a two-constituent gas within a three-dimensional, time-dependent model of the thermosphere, *Planet. Space Sci.*, *31*, 1209–1222, 1987.

Hagan, M. E., M. D. Burrage, J. M. Forbes, J. Hackney, W. J. Randel, and X. Zhang, GSWM-98: Results for migrating solar tides, *J. Geophys. Res.*, *104*, 6813–6828, 1999.

Hays, P. B., R. A. Jones, and M. H. Rees, Auroral heating and the composition of the neutral atmosphere, *Planet. Space Sci.*, *21*, 559–573, 1973.

Hecht, J. H., D. J. Strickland, A. B. Christensen, D. C. Kayser, and R. L. Walterscheid, Lower thermospheric composition changes derived from optical and radar data taken at Sondre Stromfjord during the great magnetic storm of February 1986, *J. Geophys. Res.*, *96*, 5757–5776, 1991.

Hecht, J. H., R. L. Walterscheid, M. P. Hickey, and S. J. Franke, Climatology and modeling of quasi-monochromatic gravity waves observed over Urbana, Illinois, *J. Geophys. Res.*, *106*, 5181–5195, 2001.

Hedin, A. E., Extension of the MSIS thermosphere model into the middle and lower atmosphere, *J. Geophys. Res.*, *96*, 1159–1172, 1991.

Hickey, M. P., R. L. Walterscheid, and G. Schubert, Gravity wave heating and cooling in Jupiter's thermosphere, *Icarus*, *148*, 266–281, 2000.

Isler, J. R., M. J. Taylor, and D. C. Fritts, Observational evidence of wave ducting and evanescence in the mesosphere, *J. Geophys. Res.*, *102*, 26,301–26,313, 1997.

Lindzen, R. S., Internal gravity waves in atmospheres with realistic dissipation and temperature, part I, Mathematical development and propagation of waves into the thermosphere, *Geophys. Fluid Dyn.*, *1*, 303–355, 1970.

Mayr, H. G., I. Harris, and N. W. Spencer, Some properties of upper atmospheric helium, *Rev. Geophys.*, *16*, 539–565, 1978.

Mikkelsen, I. S., and M. F. Larsen, A numerical modeling study of the interaction between the tides and the circulation forced by high-latitude plasma convection, *J. Geophys. Res.*, *96*, 1203–1213, 1991.

Mikkelsen, I. S., T. S. Jorgensen, M. C. Kelley, M. F. Larsen, and E. Pereira, Neutral winds and electric fields in the dusk auroral oval, 2, Theory and model, *J. Geophys. Res.*, *86*, 1525–1536, 1981.

Reber, C. A., and P. B. Hays, Thermospheric wind effects on the distribution of helium and argon in the Earth's upper atmosphere, *J. Geophys. Res.*, *78*, 2777–2991, 1973.

Richmond, A. D., Energy relations of atmospheric tides and their significance to approximate methods of solution for tides with dissipative forces, *J. Atmos. Sci.*, *32*, 980–987, 1975.

Richmond, A. D., and S. Matsushita, Thermospheric response to a magnetic substorm, *J. Geophys. Res.*, *80*, 2839–2850, 1975.

Straus, J. M., S. P. Creekmore, and B. K. Ching, A dynamical model of upper atmospheric helium, *J. Geophys. Res.*, *82*, 2132–2138, 1977.

Sun, Z.-P., R. P. Turco, R. L. Walterscheid, S. V. Venkateswaran, and P. W. Jones, Thermospheric response to morningside diffuse aurora: High-resolution three-dimensional simulations, *J. Geophys. Res.*, *100*, 23,779–23,793, 1995.

Taylor, M. J., M. B. Bishop, and V. Taylor, All-sky measurements of short-period waves imaged in the OI (557.7 nm), Na (589.2 nm), and near-infrared OH and O_2(0, 1) nightglow emissions during the ALOHA-93 campaign, *Geophys. Res. Lett.*, *22*, 2833–2836, 1995.

Theon, J. S., W. Nordberg, L. B. Katchen, and J. J. Horvath, Some observations of the thermal behavior of the mesosphere, *J. Atmos. Sci.*, *24*, 428–438, 1967.

Walterscheid, R. L., L. R. Lyons, and K. E. Taylor, The perturbed neutral circulation in the vicinity of a symmetric stable auroral arc, *J. Geophys. Res.*, *90*, 12,235–12,248, 1985.

Walterscheid, R. L., J. H. Hecht, R. A. Vincent, I. M. Reid, J. Woithe, and M. P. Hickey, Analysis and interpretation of airglow and radar observations of quasi-monochromatic gravity waves in the upper mesosphere and lower thermosphere over Adelaide, Australia (35°S, 138°E), *J. Atmos. Sol. Terr. Phys.*, *61*, 461–478, 1999.

Walterscheid, R. L., J. H. Hecht, F. T. Djuth, and C. A. Tepley, Evidence of reflection of a long-period gravity wave in observations of the nightglow over Arecibo on May 8–9, 1989, *J. Geophys. Res.*, *105*, 6927–6934, 2000.

M. P. Hickey, Department of Physics and Astronomy, Clemson University, Clemson, SC 29634-0978, USA.

R. L. Walterscheid, Space Science Applications Laboratory, The Aerospace Corporation, 2350 East El Segundo Boulevard, El Segundo, CA 90245-4691. (Richard.Walterscheid@aero.org)

(Received April 3, 2001; revised June 20, 2001;
accepted June 25, 2001.)